Strahlenther Onkol
https://doi.org/10.1007/s00066-021-01828-8

ORIGINAL ARTICLE

Postsurgical geometrical variations of tumor bed and brainstem during photon and proton therapy for pediatric tumors of the posterior fossa: dosimetric impact and predictive factors

Stefania Volpe[1,2] · Pierre-Yves Bondiau[3] · Line Claude[4] · Audrey Claren[3] · Laetitia Padovani[5] · Hamza AlGhamdi[3,6] · Gwenaëlle Duhil De Benaze[7] · Lucas Opitz[8] · Guillaume Baudin[9] · Catherine Dejean[3] · Daniel Maneval[3] · Barbara Alicja Jereczek-Fossa[1,2] · Jérôme Doyen[3]

Received: 5 January 2021 / Accepted: 4 July 2021

Abstract

Purpose Brainstem radionecrosis is an important issue during the irradiation of tumors of the posterior fossa. The aim of the present study is to analyze postsurgical geometrical variations of tumor bed (TB) and brainstem (BS) and their impact on dosimetry.

Methods Retrospective collection of data from pediatric patients treated at a single institution. Availability of presurgical magnetic resonance imaging (MRI) was verified; availability of at least two postsurgical MRIs was considered a further inclusion criterion. The following metrics were analyzed: total volume, Dice similarity coefficient (DSC), and Haudsdorff distances (HD).

Results Fourteen patients were available for the quantification of major postsurgical geometrical variations of TB. DSC, HD max, and HD average values were 0.47 (range: 0.08;0.76), 11.3 mm (7.7;24.5), and 2.6 mm (0.7;6.7) between the first and the second postoperative MRI, respectively. Postsurgical geometrical variations of the BS were also observed. Coverage to the TB was reduced in one patient (D95: –2.9 Gy), while D2 to the BS was increased for the majority of patients. Overall, predictive factors for significant geometrical changes were presurgical gross tumor volume (GTV) > 33 mL, hydrocephaly at diagnosis, Luschka foramen involvement, and younger age (≤ 8 years).

Conclusion Major volume changes were observed in this cohort, with some dosimetric impact. The use of a recent co-registration MRI is advised. The 2–3 mm HD average observed should be considered in the planning target volume/planning organ at risk volume (PTV/PRV) margin and/or robust optimization planning. Results from wider efforts are needed to verify our findings.

Keywords Protontherapy · Surgical bed · Central nervous system tumors · Pediatric radiation oncology · Treatment planning optimization

J. Doyen is the author responsible for the statistical analysis.

✉ Stefania Volpe, M.D.
stefania.volpe@ieo.it

✉ Jérôme Doyen, M.D., Ph.D.
jerome.doyen@nice.unicancer.fr

[1] Division of Radiation Oncology, IEO, European Institute of Oncology IRCCS, Milan, Italy

[2] Department of Oncology and Hemato-Oncology, University of Milan, Milan, Italy

[3] Antoine Lacassagne Centre, Department of Radiation Oncology, Fédération Claude-Lalanne, University of Côte d'Azur, Nice, France

[4] Department of Radiation Oncology, Léon Bérard Centre, Lyon, France

[5] Oncology Radiotherapy Department, CRCM Inserm, UMR1068, CNRS UMR7258, AMU UM105, Genome Instability and Carcinogenesis, Assistance Publique des Hôpitaux de Marseille, Aix-Marseille University, Marseille, France

[6] Oncology Center, King Faisal Medicao City for Southern Region, Abha, Saudi Arabia

[7] Pedatric Oncology, Archet Hospital, Nice, France

[8] Antoine-Lacassagne Centre, Department of Anesthesiology, University of Côte d'Azur, Nice, France

[9] Antoine-Lacassagne Centre, Department of Radiology, University of Côte d'Azur, Nice, France

Published online: 05 August 2021

Abbreviations

BS	Brainstem
CNS	Central nervous system
CT	Computed tomography
CTV	Clinical target volume
DICOM	Digital Imaging and Communication in Medicine
DSC	Dice similarity coefficient
EPTN	European Particle Therapy Network
GTV	Gross tumor volume
HD	Hausdorff distance
IQR	Interquartile range
LET	Linear energy transfer
MRI	Magnetic resonance imaging
NTCP	Normal tissue complication probability
OAR	Organ at risk
PF	Posterior fossa
PRV	Planning organ at risk volume
PT	Proton therapy
PTV	Planning target volume
ROI	Region of interest
RT	Radiotherapy
RBE	Relative biological effectiveness
SOBP	Spread-out Bragg peak
TB	Tumor bed
TPS	Treatment planning system

Introduction

Central nervous system (CNS) cancers are the most common solid tumors in children, accounting for up to 25% of childhood malignancies [1–3]. Of those, approximatively two thirds originate in the posterior fossa (PF), which is the most involved intracranial compartment in the 0–4 years age group [3, 4]. While photon-based radiotherapy (RT) has a well-established role in the treatment of these patients, the more recent advent of proton therapy (PT) holds the promise to further improve the therapeutic ratio in children diagnosed with CNS cancers. Consistently, a growing body of evidence has suggested a decrease in treatment-related morbidities, including lower rates of secondary malignancies [5, 6] and less severe impairments in the cognitive and psychosocial domains [7–10]. The rationale for PT use in pediatric neuro-oncology lies in the physical properties of particles (namely lower entrance path dose and absence of exit dose), which translates into a significantly reduced integral dose.

Nevertheless, the higher relative biological effectiveness (RBE) of protons as compared to photons has been associated with a potentially higher risk of severe treatment-related morbidities [11]. Specifically, the progressive increase in linear energy transfer (LET) throughout the spread-out Bragg peak (SOBP) may account for the so-called end-of-beam-path toxicity, which is believed to be critical for serial structures such as those belonging to the CNS [12, 13]. Available evidence suggests that endothelial cells at the edge of the SOPBP could experience an enhanced rate of apoptotic phenomena, leading to demyelination and injury to the brainstem (BS), with the pons being the most susceptible area, especially in younger children [14, 15]. While some series have reported a higher prevalence of BS injury following PT as compared to photons [16–20], it is unclear whether this difference can be explained—either partially or completely—by variations in the RBE/LET ratio. In particular, two recent modeling studies have underlined that the location of the primary tumor within the brain and interpatient variability in radiosensitivity may play a relevant role in determining the onset of treatment-related toxicity [21, 22]. In order to refine the therapeutic index of PT [23], conclusions from a recent expert workshop convened by the National Cancer Institute have underlined the need to reconsider the currently accepted dose/volume constraints, to optimize treatment planning around LET (or, ideally, around RBE), and to refine radiobiological knowledge on patient-specific biomarkers of radiation injury susceptibility [21, 24]. Arguably, a comprehensive understanding of these clinical and dosimetric variables would result in the development of dedicated normal tissue complication probability (NTCP) models for BS injury risk stratification in children with tumors of the PF.

Further complexity may be introduced by possible intrapatient variability over time. A preliminary body of evidence from retrospective series on adult patients treated with RT for resected brain metastases has suggested that the modification of surgical cavities may be more relevant than previously expected on the sole basis of qualitative everyday clinical experience [25–27]. Specifically, surgical cavity dynamics may lead to substantial volumetric and positional modifications even prior to the beginning of RT, with a potentially significant effect on CTV delineation and subsequent dose distribution. Moreover, it is sufficiently straightforward to hypothesize that nearby organs at risk (OARs) may undergo modifications as well, especially when located in close proximity to the surgical cavity. Changes in TB and OAR geometries are even more critical during PT [28, 29], due to the sensitivity of proton dose distribution to geometrical changes [30, 31], and could have a clinically meaningful role in the occurrence of BS radionecrosis.

To address these open questions, we performed a retrospective analysis of pediatric patients treated at the Centre Antoine Lacassagne (Nice, France) for tumors of the PF (medulloblastoma and ependymoma), aiming to:

- quantify TB and BS modifications, if any, across a longitudinal series of postsurgical/pre-RT MRIs;

- verify whether geometrical changes for the TB and the BS are associated with any modifications in TB coverage and dose to the BS;
- to identify clinical predictive factors for anatomical changes.

Patients and methods

Patient selection

Pediatric patients treated with adjuvant RT for tumors of the PF at the Centre Antoine Lacassagne (Nice, France) between 2000 and 2019 were eligible for the analysis. Inclusion criteria were: 1) patients aged less than or equal to 18 years old at the time of diagnosis; 2) histologically confirmed diagnosis of malignant tumors of the PF; 3) accessibility to digitalized medical records for the retrieval of clinical information including, but not limited to, patient demographics, tumor characteristics, and treatment-related features; 4) availability of DICOM (Digital Imaging and Communication in Medicine) files from at least two postsurgical, pre-RT gadolinium-enhanced MRIs per child; 5) availability of treatment planning data (i.e., RT.struct and RT.dose files); 6) availability of written parental consent to RT treatment delivery and to the anonymized use of clinical metadata for clinical research purposes.

Both proton-based and composite proton/photon RT treatments were accepted. The following clinical data were retrieved: patients' baseline characteristics (gender, age at diagnosis, symptomatic onset of disease, surgical complications) and treatment features (type of RT, fractionation, total dose, CSI administration, chemotherapy administration and timing), together with tumor-related parameters (i.e., histology).

In compliance with the European General Data Protection Regulation, the present study was approved by the French National Health Authorities (registration number: 1809080120). All families received written information on the study and gave their explicit consent to the anonymous use of patient data for research purposes.

CT simulation protocol

All patients underwent CT simulation at the Centre Antoine Lacassagne (Nice, France); a DISCOVERY scanner (General Electric Healthcare, Chicago, IL, USA) was used in all cases. Internal protocols with predefined parameters were adopted for image acquisition; overall, median slice thickness was 1.25 mm (interquartile range, IQR: 0.31 mm). Median reconstruction diameter (namely the diameter in mm of the region from which data were used for image reconstruction) was 480 mm (IQR: 442.5–500). None of the patients were injected with iodinated contrast agent. Other than a thermoplastic mask, simulation set-up included a BlueBAG™ Vacuum cushion (Elekta Atlanta, GA, USA) to facilitate reproducible positioning for all patients.

Image registration and ROI contouring

Patients' MRIs were retrieved from electronic archives and imported into the RayStation (RaySearch Laboratories, Stockholm, Sweden) treatment planning system (TPS), version 6.1.1.2 for semi-automated rigid image registration [32]. The CT simulation scan was set as the primary image; accuracy of the registration was verified by systematic pointwise comparison to bony anatomy in the axial, sagittal, and coronal planes. Revision by an expert dedicated radiologist (GB) was required as needed. Subsequently, a manual MRI-based segmentation was performed for the TB and the BS at all the available timepoints. Delineation of the presurgical gross tumor volume (GTV), resection cavity with residual tumor (if any), and BS was carried out on contrast-enhanced T1-weighted MRI sequences; surrounding edema was identified as hyperintensity in FLAIR and T2-weighted sequences.

For the analysis, both TBs and BSs were contoured at all available timepoints.

Histologically negative tissue defects from surgical procedure(s) were not included in the GTV. The anatomical borders of the BS were defined according to the European Particle Therapy Network (EPTN) guidelines [33].

Statistical analysis and image metrics

Categorical data were presented as percentage and frequency; the interquartile range (IQR) was calculated for continuous variables. The Mann–Whitney U test was used to compare continuous variables and the chi-square test for qualitative variables. The following factors were tested as potential predictive factors for TB or BS changes: age (>8 years vs. ≤8 years), GTV (>33 mL vs. ≤33 mL), hydrocephaly at diagnosis, surgical complications, Luschka foramen involvement, Magendie foramen involvement, prepontic cistern involvement, pons infiltration, medulla oblongata infiltration, degree of tumoral adherence to the BS (>90° vs. ≤90°). The cut-off values for patients' age and tumor volume were chosen based on the median of variables. Due to the small sample size, *p*-values in this study only reflect the individual comparisons and have not been adjusted for the total number of tests.

To provide a comprehensive quantitative assessment of the ROI modifications over time, the following metrics were selected:

1. *Total ROI volume:* volumetric evaluation of GTV, TB, and BS was performed in each patient at all the available timepoints using the RayStation (RaySearch Laboratories, Stockholm, Sweden) TPS [34].
2. *Dice similarity coefficient (DSC):* also known as the Sørensen–Dice index, it is a statistic used to gauge the similarity between two samples (A and B), defined as:

$$DSC = \frac{2|A \cap B|}{|A|+|B|}$$

As a measure of spatial overlap, DSC values may range from 0 (absence of spatial overlap) to 1 (complete overlap) [35].
3. *Hausdorff distances (HDs):* these assesses the distance in pixels between two non-empty regions. Specifically, the maximum and average HDs can be defined to characterize the maximum and mean distances between two regions (two ROIs in our specific case): the smaller the distances, the higher the overlap between the considered contours [35, 36].

A visual representation of the above-described metrics is provided in Fig. 1.

Both the DSCs and the HDs were computed using 3D Slicer version 4.10.2, an open-source software platform for medical imaging informatics, processing, three-dimensional visualization, and quantitative analysis [37].

For each patient, DICOM files from the CT scan and associated RT.struct files for ROIs were exported from RayStation TPS to 3D Slicer. Subsequently, metrics were extracted by the 3D Slicer Segment Comparison tool (SlicerRT extension Revision bb256e2).

Dosimetric parameters

The following dosimetric parameters were retrieved for both the TB and the BS at each time point using the original treatment plan: D99, D98, D95, Average Dose, D50, D2 and D1 (with D99, D98, D95, D50, D2 and D1 indicating the dose to the 99%, 98%, 95%, 50%, 2% and 1% of the volumes of interest, respectively). All calculations were performed using RayStation (RaySearch Laboratories, Stockholm, Sweden).

Results

Overall, 14 patients were considered eligible for the analysis; prior to surgery, all of them had undergone a cerebrospinal fluid analysis and a MRI of the spine and brain. Patients were equally distributed per gender; median age at the time of diagnosis was 8.2 years (range: 1.2;18.3), with the youngest and the oldest patients being 1.2 and 18.1 years old, respectively. All but two patients had received radical surgery, postoperative residual volume was < 1.5 cm^3 in both cases. Relevant clinical information is summarized in Table 1. Data on anatomical involvement of PF sub-structures before neurosurgery are provided in Supplementary Material 1.

Overall, 12 preoperative and 39 postoperative MRIs were available for the analysis. The median delay between surgery and postoperative MRI was 46 days (range: 2–154 days). Specifically, 11 MRIs were performed between postoperative days 1 and 7 (first postoperative MRIs), 16 between days 8 and 90 (second postoperative MRIs),

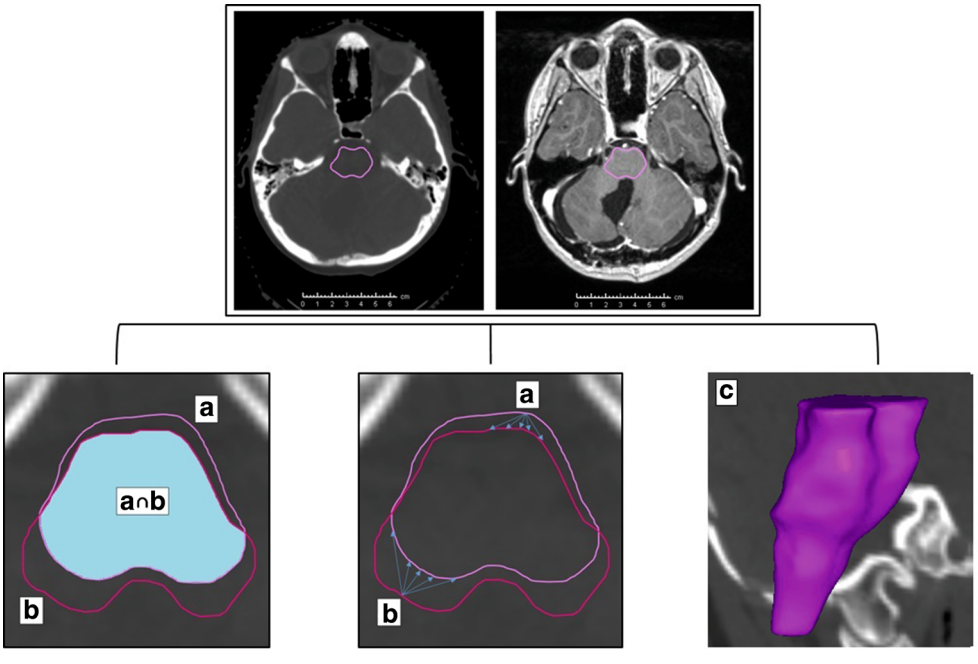

Fig. 1 Graphical representation of the Dice coefficient (*a*), Hausdorff distance (*b*) and volume (*c*) metrics. The violet and pink lines indicate the BS. In *a*, the light blue region show the overlap between the BS at two different time points, as measured by the Dice coefficient; the arrows in *b* indicate the maximum and minimum Hausdorff distances between the contours

Table 1 Patient- and treatment-related characteristics

n (%)	
Age at the time of diagnosis: median (range), years	8.17 (1.23–18.32)
Gender	
Male	7 (50)
Female	7 (50)
Primary tumor	
Medulloblastoma	12 (86)
Ependymoma	2 (14)
Neurological presentation symptoms	
Yes	14 (100)
No	0 (0)
Neurological presentation symptoms, detail	
Headache	10 (71)
Nausea	10 (71)
Ataxia	8 (57)
Apraxia	2 (14)
Visual impairment	2 (14)
Neglect	1 (7)
Hemi-syndrome	1 (7)
Night terrors	1 (7)
Hydrocephaly at diagnosis	
Yes	7 (50)
No	7 (50)
Surgical complications	
Yes	5 (35)
No	9 (65)
Presence of residual disease after surgery	
Yes	2 (14)
No	12 (86)
Chemotherapy administration	
Yes	11 (79)
Adjuvant only	9
Adjuvant + concomitant	2
No	3 (21)
CSI	
Yes	12 (86)
No	2 (14)
CSI dose: mean (SD), Gy	32.4 (5.4)
Type of RT	
Exclusive proton RT	2
Exclusive photon RT	3
Photon and proton boost	9
Proton radiotherapy dose: median (IQR), Gy	18 (12–30)

CSI craniospinal irradiation, *IQR* interquartile range, *RT* radiotherapy, *SD* standard deviation

Table 2 Dice coefficient (DSC) and Hausdorff distance (HD) variations for the tumor bed and brainstem

	1st versus 2nd MRI	1st versus 3rd MRI
Tumor bed		
Median DSC	0.47 (0.08;0.76)	0.42 (0.04;0.69)
Median HD average	2.6 mm (0.7;6.7)	2.6 mm (0.5;11)
Median HD max	11.3 mm (7.7;24.5)	12.1 mm (8.1;40.2)
Brainstem		
Median DSC	0.64 (0.2;0.82)	0.58 (0.16;0.77)
Median HD average	2 mm (0.4;3.3)	2.2 mm (0.5;9.3)
Median HD max	8.5 mm (4.5;14)	10.6 mm (7.9;27.1)

DSC Dice coefficient, *HD* Hausdorff distance, *MRI* magnetic resonance imaging

and 12 between 91 and 188 days after surgery (third postoperative MRIs). Median delays between imaging and the start of RT were as following: 111 days (range: 28–159) for the first postoperative MRI, 22 days (140 before to 85 days after the start of RT) for the second, and 21 days (91 before to 23 days after the start of RT) for the third MRI. For ependymoma, prescription doses were 54 Gy to the TB plus a 5-mm margin; the treatment was continued with a sequential boost up to 59.4 Gy only if the patient had a good neurological performance after surgery. Patients diagnosed with intermediate- or high-risk medulloblastoma were treated to the craniospinal axis until 23.4 Gy or 36.0 Gy, respectively, and then boosted up to 54 Gy to either the tumor bed (intermediate-risk; 7 patients) or the whole PF (high-risk; three patients). Only one patient was treated with a bifractionated regimen until 68 Gy. Due to logistic constraints, CSI was realized with photons in all cases.

Tumor bed modifications

No further relevant absolute volume modifications were found at the second and third imaging re-evaluations.

The quantification of DSC between the TB contours indicated that surgical cavity geometry underwent significant modifications across all the considered timepoints, with a median overlap of 0.47 (range: 0.08;0.76) between the first and the second postoperative MRIs, and of 0.42 (range: 0.04;0.69) between the first and the third postoperative MRIs.

The HD max underwent longitudinal modifications, with a median value of 11.3 mm (range: 7.7–24.5) when comparing TBs at the first and second timepoints, and 12.1 mm (range: 8.1–40.2) when the calculation was performed between the first and third MRIs.

The HD average varied as well, both when comparing the first and the second MRIs (median of 2.6 mm,

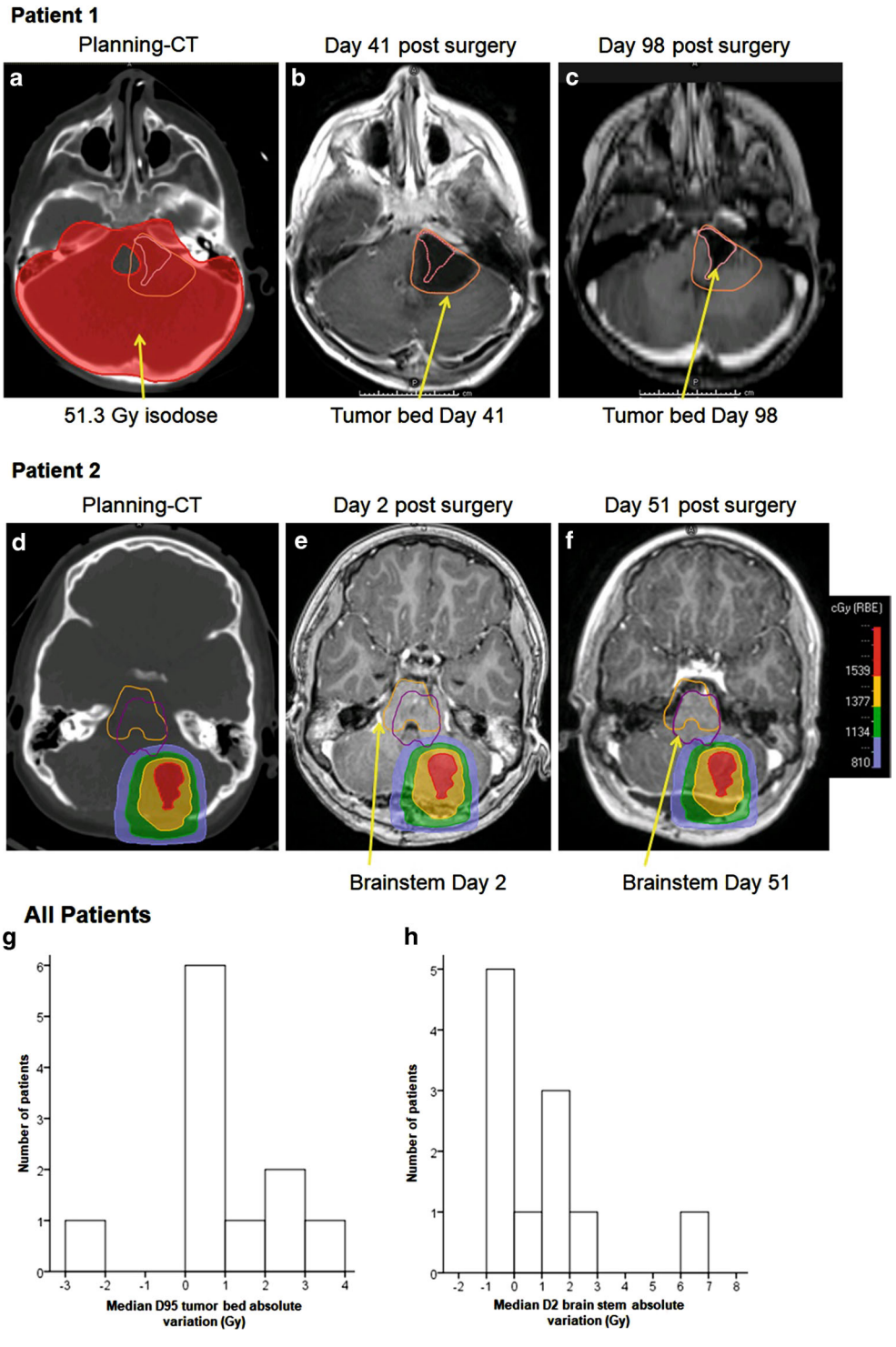

Fig. 2 Patient 1: Treatment plan of a patient with medulloblastoma, boosted up to 54 Gy on the posterior fossa (photon + proton irradiation); the 51.3 Gy isodose (*red*) is depicted in **a**, the tumor bed (TB) 41 days after surgery in **b**, and the TB 98 days after surgery in **c**. Patient 2: Treatment plan of a patient with medulloblastoma, boosted up to 54 Gy in the TB (with proton irradiation); the planning CT is depicted in **d**, the brainstem at day 2 after surgery in **e**, and the brainstem on day 51 after surgery in **f**. All patients: median D95 absolute variations of the TB (Gy; **g**) and median D2 absolute variation of brainstem (Gy; **h**)

range: 0.7–6.7 mm), and the first and third MRIs (median of 2.6 mm, range: 0.5;11 mm).

A summary of geometric changes is provided in Table 2, while Fig. 2 gives a graphical representation of TB modifications for one patient (Patient 1).

Brainstem modifications

We did not observe any significant postoperative modifications in the BS volume, with its median value remaining constant over time across all the considered MRIs. Only a minor reduction was noted at the third postoperative MRI

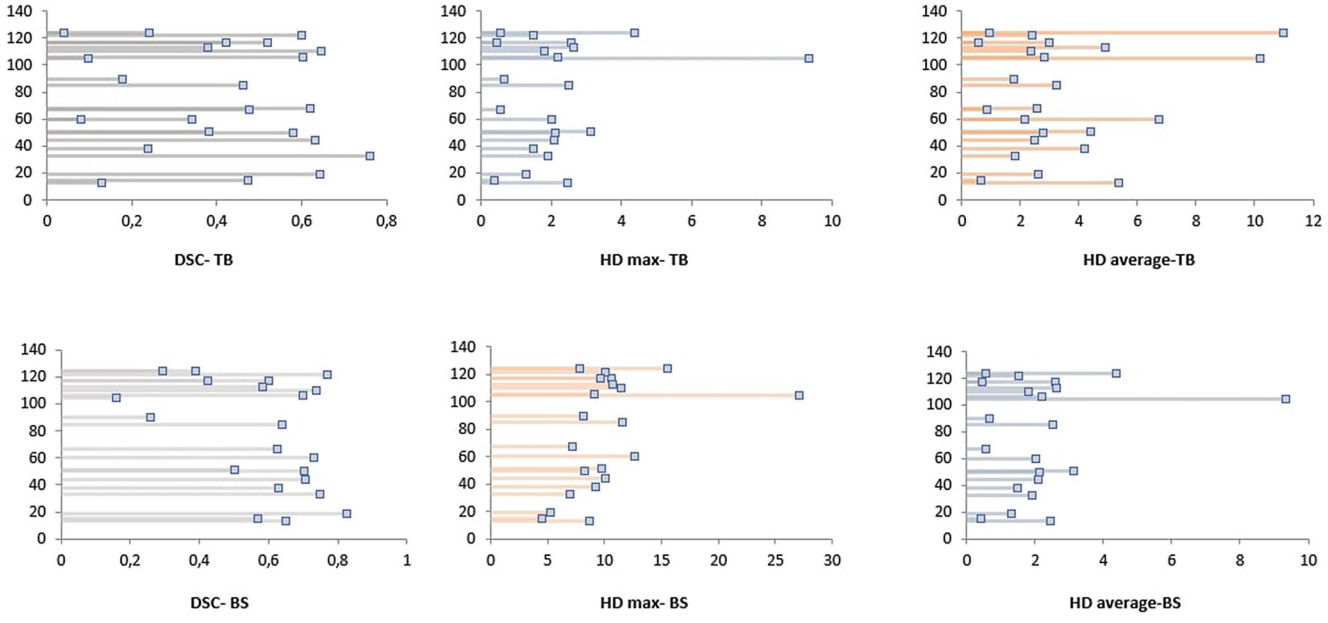

Fig. 3 Swimmers plots for the variations of Dice coefficient and maximum and average Hausdorff distances over time. X axis: metric of interest; y axis: delay between first postoperative MRI and subsequent MRI

assessment (median volume = 15.7 ml vs. 16.6 ml at the second postoperative MRI, $p = 0.9$).

However, relevant changes were noted between the first and second postoperative MRIs (median DSC = 0.64, 0.2;0.82). An even more significant reduction in the DSC was recorded when the second and the third postoperative MRIs were compared (DSC = 0.58, 0.16;0.77).

The HD max showed also major modifications, with a median value of 8.5 mm (4.5;14) between the first and second postoperative MRIs, and of 10.6 mm (7.9;27.1) between the first and third imaging evaluations. The median HD average was 2 mm (0.4;3.3) and 2.2 mm (0.5;9.3) between the first and second, and between the first and third postoperative MRI, respectively.

A summary of geometric changes is given described in Table 2. Fig. 2 provides an example of BS modifications for one of the patients included in the analysis (Patient 2).

A comprehensive overview of geometrical modifications for both the TB and the BS is provided in Fig. 3. Globally, our findings confirm a tendency towards a decrease in the DSC, and a consensual increase in the Hausdorff metrics over time.

Dosimetric impact of anatomical modifications

The dosimetric impact of the anatomical changes for clinically relevant treatment plan parameters is reported in Table 3 and Fig. 2.

In this cohort the geometric changes did not affect TB coverage, except for in one patient diagnosed with high-risk medulloblastoma who received irradiation to the whole PF. Specifically, anatomical changes determined a reduction of 2.9 Gy of the D95% (Fig. 2, Patient 1). Conversely, all other patients included in the analysis underwent an increase in TB coverage (Fig. 2, All patients).

The impact of geometric modification on dosimetry was more significant for the BS (Fig. 2, All patients) Three patients presented a 1–2 Gy increase of D2, 1 patient a 2 Gy increase, and 1 patient a 6 Gy increase (Fig. 2, Patient 2). Of these, four patients received a proton boost to the TB,

Table 3 Variations in dose distribution for tumor bed and brainstem coverages (absolute and relative)

Tumor bed coverage	Absolute variation (Gy)	Relative variation (%)
Median D99% variation	+1.4 (–1.3; +7)	+6.7 (–2.7; +36.1)
Median D98% variation	+1.1 (–1.7; +7.7)	+5.6 (–3.3; +33.8)
Median D95% variation	+0.3 (–2.9; +3.9)	+1.7 (–5.6; +16.1)
Median average dose variation	+0.09 (–0.5; +0.7)	+0.5 (–0.9; +2.9)
Brainstem		
Median D50% variation	+1.3 (–0.9; +3.8)	+11.7 (–1.8; +228.9)
Median D2% variation	+0.6 (–0.5; +6.1)	+0.9 (–0.9; +147.1)
Median D1% variation	+0.5 (–0.4; +6.3)	+0.7 (–1.1; +126.5)

Table 4 Predictive factors for anatomical variations, univariate analyses

	DSC first MRI vs. second MRI	HD max first MRI vs. second MRI (mm)	HD average first MRI vs. second MRI (mm)	DSC first MRI vs. third MRI	HD max first MRI vs. third MRI (mm)	HD average first MRI vs. third MRI (mm)
Tumor bed						
Age	$p = 0.07$	$p = 0.07$	$p = 0.1$	$p = 0.6$	$p = 0.4$	$p = 0.1$
>8 years						
≤8 years						
GTV	$p = 0.3$	$p = 0.4$	*$p = 0.02$*	$p = 0.9$	$p = 0.2$	*$p = 0.01$*
33 mL			2.6 [1.8;4.4]			3.2 [2.4;10.9]
≤33 mL			2.5 [0.7;6.7]			1.8 [0.5;2.6]
Hydrocephaly at diagnosis	$p = 0.1$	*$p = 0.01$*	*$p = 0.001$*	$p = 0.6$	$p = 0.09$	*$p = 0.01$*
Yes		15 [7.7;24.5]	4.2 [0.7;6.7]			3.1 [2.4;10.9]
No		10 [7.9;12]	2.1 [0.8;2.8]			1.8 [0.5;2.8]
Luschka involvement	*$p = 0.04$*	$p = 0.6$	$p = 0.8$	$p = 0.2$	$p = 0.6$	$p = 0.7$
Yes	0.47 [0.08;0.6]					
No	0.63 [0.4;0.76]					
Magendie involvement	$p = 0.2$	$p = 0.9$	$p = 0.2$	$p = 0.3$	$p = 0.8$	$p = 0.5$
Yes						
No						
Time between surgery and the RT (start)	$p = 0.6$	$p = 0.2$	$p = 0.4$	$p = 1.0$	$p = 1.0$	$p = 0.9$
Brainstem						
Age	$p = 0.9$	*$p = 0.02$*	$p = 0.4$	$p = 0.6$	*$p = 0.02$*	$p = 0.2$
>8 years		7.1 [4.5;9.7]			9.3 [7.9;10.7]	
≤8 years		9.6 [7.9;13.9]			11.5 [9.7;27.1]	
GTV	$p = 0.8$	$p = 0.4$	$p = 0.7$	$p = 0.4$	$p = 0.3$	*$p = 0.01$*
33 mL						2.5 [1.5;9.3]
≤33 mL						0.6 [0.5;2]
Hydrocephaly at diagnosis	$p = 0.1$	$p = 0.8$	$p = 1$	$p = 0.8$	$p = 0.09$	*$p = 0.01$*
Yes						2.5 [1.5;9.3]
No						0.6 [0.5;2.2]
Luschka foramen involvement	$p = 1.0$	$p = 0.3$	$p = 1.0$	$p = 0.9$	$p = 0.9$	$p = 1.0$
Yes						
No						
Magendie foramen involvement	$p = 0.3$	$p = 0.7$	$p = 0.4$	$p = 0.2$	$p = 0.1$	$p = 0.5$
Yes						
No						
Time between surgery and the RT (start)	$p = 0.4$	$p = 0.6$	$p = 0.3$	$p = 0.6$	$p = 0.9$	$p = 0.9$

DSC Dice coefficient, *GTV* gross tumor volume, *HD* Hausdorff distance, *MRI* magnetic resonance imaging
The indicated *p*-values reflect individual comparisons and have not been adjusted for the total number of tests

while the fifth underwent a photon-based treatment. The increase in D2 exceeded 54 Gy in two cases.

Clinical factors associated with anatomical modifications

Several factors correlated with greater anatomical modifications: GTV > 33 mL, hydrocephaly at diagnosis, and Luschka foramen involvement (Table 4). Pre-pontic cistern involvement, pons and medulla oblongata infiltration, and the degree of tumoral adherence to the BS (>90° vs. ≤90° around BS) did not show any correlation with geometrical modification assessed per the DSC, HD max, HD average, and volume metrics in our series.

Discussion

The current work investigates the value of four metrics, namely the volume, the DSC, the maximum, and the average HDs in quantifying postsurgical, pre-RT modifications of the CTV and the BS as compared to presurgical volumes. To the best of our knowledge, this is the first study in pediatric neuro-oncology to implement the use of novel descriptors to investigate the still unanswered questions regarding structural modifications in response to neurosurgery, and their relative impact on dosimetry. Overall, we observed a trend towards a decrease of the TB volume over time; these modifications were consistent with a reduction in the DSC, as well as an increase in the median HD max value, showing the existence of geometrical changes. Median HD average for TB was 2.6 mm. Notably, maximum overlaps were 0.76 and 0.69 between the first and the second, and the first and the third MRI as measured per the DSC, which suggests that relevant modifications in the DSC values occurred in all patients included in our cohort.

Modifications were also observed for the BS, whose volume showed a statistically significant decrease in the postsurgical MRIs; the DSC, HD max, and HD average had a similar evolution profile to the TB, with relevant anatomical modifications.

The dosimetric analysis showed that anatomical changes translate into a relevant effect on dose distribution: dosimetric changes regarding TB coverage show increased values, except for in one patient for whom the coverage decreased. When considering the dose to the BS, we noted more impact on D2 max values, meaning that the timing of MRI is of importance to have the greatest dosimetric accuracy.

Despite the small sample size, variations of TB and BS were frequent, and our results strongly suggest to include a recent MRI at the time of RT planning. Of note, significant modification of both the TB and the BS were observed in one case (Patient 1) between the postoperative days 41 and 98 after surgery. As most patients are generally receiving PF irradiation at postsurgical day 98, this may suggest that volumetric modifications can still be present during treatment. Consequently, in-treatment MRIs may be useful to operate adaptive-planning strategies in these patients. According to the results of our work, patients with larger tumors (>33 ml), hydrocephaly at diagnosis, Luschka foramen involvement, and younger age (≤8 years) have the highest probability of undergoing significant geometrical changes.

This issue is specifically relevant for PT, as described in a recent work by Fjæra et al. exploring the impact of tumor location on LET and biological dose to the BS during intensity-modulated PT [38]. The authors could demonstrate that distant tumor volumes correlated with high dose-averaged LET values to the BS, despite the impact of dose-averaged LET values being more relevant in case of close proximity between the BS and the GTV.

A recently published work by Acharya et al. [39] on 73 pediatric tumors of both brain and non-brain origin treated with PT has underlined the importance of in-treatment MRI to allow adaptive re-planning according to CTV modifications. Specifically, 11/73 patients (15%) showed significant anatomical changes, leading to potential target undercoverage (7 patients) or unjustified excess in the delivered dose to the OARs (4 patients). Despite several differences existing between our series and the one by Acharya et al. (i.e., extracranial cancers included), the two works highlight the role of MRI in assessing pre- and in-treatment modifications to optimize the therapeutic ratio of PT in pediatric cancers. Interestingly, a consistent association between clinically meaningful anatomical changes and younger age was demonstrated in both series, which calls for further investigation to identify patient-related characteristics at the time of treatment planning and delivery.

We acknowledge that results of our work are limited by its retrospective nature and small sample size. Admittedly, it was not possible to retrieve all MRIs, and prescription doses were not homogenous across the considered cohort. Also, we recognize varying time intervals between MRIs, which could at least partially impair the generalizability of our findings. Another potentially relevant factor is that most of the patients diagnosed with medulloblastoma were treated according to the schedule of the PNET-HR+5 phase II trial (NCT00936156), which accounts for the relatively long interval between surgery and the start of RT, while the current approach prioritizes the start of adjuvant RT in this clinical setting. Despite these limitations advocating for a cautious interpretation, our results are the first to prompt a comprehensive investigation on the dosimetric impact of anatomical variations of the TB and closely located organs at risk.

Although the metrics used in the present work are not widely known among clinicians, we support their diffusion at least in the setting of clinical research. Moreover, both the DSC and the HDs can easily be calculated by free user-friendly tools which do not require dedicated computational resources or informatics knowledge of any kind. If the above-mentioned metrics were applied to future efforts, a more complete body of knowledge would be available to build multi-dimensional models of surgical cavity kinetics, including clinical, imaging, dosimetric, and quantitative parameters for target coverage optimization. In our opinion, data on BS kinetics could be of use for the development of dedicated NTCP models for children diagnosed with tumors of the PF treated with PT.

To provide more accurate effect estimates and predictive factors for anatomical changes, further retrospective research on other cohorts is warranted, and should be envisioned as a more solid benchmark for prospective efforts. In this regard, the setting of a systematically structured plan for postoperative MRI would allow for more consistent longitudinal comparisons of imaging data. Moreover, investigations on other brain structures (i.e., the cerebellum, BS substructures) could be informative, as well as the testing of additional patient- and tumor-related parameters (i.e., age, clinical presentation at diagnosis, response to chemotherapy, histology). Additionally, other studies should be performed to assess the effect of RT on anatomical variations of the TB, which we could not perform due to the unavailability of in-treatment MRIs.

In conclusion, our work could demonstrate the existence of relevant geometric variations of TB and BS. This represents a concrete step towards the prediction of TB and BS modifications in response to neurosurgery in children treated for tumors of the PF. If confirmed by a more robust body of knowledge, this information should be considered and become part of routine PT planning. The 2–3 mm modification in HD average should be considered when giving PTV/PRV margins and/or performing treatment planning with robust optimization procedures. This is specifically true when MRI imaging is not available and/or when reasons to expect significant volumetric modifications in the TB are present; however, these evaluations require caution, and should be performed on an individual patient basis. Our recommendation is to perform the co-registration MRI as close as possible to the CT simulation scan for treatment planning purposes (i.e., 10–14 days), and to repeat MRI 2 weeks after the start of RT, which confirms the indication by Acharaya et al. [39]. Also, we suggest adopting all available measurements to minimize geometrical uncertainty (i.e., correct patient positioning) in addition to robust plan optimization and margining. Re-scanning and iterative adaptive planning may be considered as well, especially in case of large GTVs > 33 mL, hydrocephaly at diagnosis, Luschka foramen involvement, and in patients of younger age (≤ 8 years).

Supplementary Information The online version of this article (https://doi.org/10.1007/s00066-021-01828-8) contains supplementary material, which is available to authorized users.

Acknowledgements Stefania Volpe MD was partially supported by the Italian Ministry of Health with *Progetto di Eccellenza*, and is a PhD student within the European School of Molecular Medicine (SEMM).

Conflict of interest S. Volpe, P.-Y. Bondiau, L. Claude, A. Claren, L. Padovani, H. AlGhamdi, G. Duhil De Benaze, L. Opitz, G. Baudin, C. Dejean, D. Maneval, B.A. Jereczek-Fossa, and J. Doyen declare that they have no competing interests.

References

1. Patel AP, Fisher JL, Nichols E, Abd-Allah F, Abdela J, Abdelalim A et al (2019) Global, regional, and national burden of brain and other CNS cancer, 1990–2016: a systematic analysis for the Global Burden of Disease Study 2016. Lancet Neurol 18:376–393. https://doi.org/10.1016/S1474-4422(18)30468-X
2. Bray F, Ferlay J, Soerjomataram I, Siegel RL, Torre LA, Jemal A (2018) Global cancer statistics 2018: GLOBOCAN estimates of incidence and mortality worldwide for 36 cancers in 185 countries. CA Cancer J Clin 68:394–424. https://doi.org/10.3322/caac.21492
3. Johnson KJ, Cullen J, Barnholtz-Sloan JS, Ostrom QT, Langer CE, Turner MC et al (2014) Childhood brain tumor epidemiology: a brain tumor epidemiology consortium review. Cancer Epidemiol Biomarkers Prev 23:2716–2736. https://doi.org/10.1158/1055-9965.EPI-14-0207
4. D'Arco F, Khan F, Mankad K, Ganau M, Caro-Dominguez P, Bisdas S (2018) Differential diagnosis of posterior fossa tumours in children: new insights. Pediatr Radiol 48:1955–1963. https://doi.org/10.1007/s00247-018-4224-7
5. Chung CS, Yock TI, Nelson K, Xu Y, Keating NL, Tarbell NJ (2013) Incidence of second malignancies among patients treated with proton versus photon radiation. Int J Radiat Oncol Biol Phys 87:46–52. https://doi.org/10.1016/j.ijrobp.2013.04.030
6. Bekelman JE, Schultheiss T, Berrington De Gonzalez A (2013) Subsequent malignancies after photon versus proton radiation therapy. Int J Radiat Oncol Biol Phys 87:10–12. https://doi.org/10.1016/j.ijrobp.2013.05.016
7. Yock TI, Bhat S, Szymonifka J, Yeap BY, Delahaye J, Donaldson SS et al (2014) Quality of life outcomes in proton and photon treated pediatric brain tumor survivors. Radiother Oncol 113:89–94. https://doi.org/10.1016/j.radonc.2014.08.017
8. Kahalley LS, Ris MD, Grosshans DR, Okcu MF, Paulino AC, Chintagumpala M et al (2016) Comparing intelligence quotient change after treatment with proton versus photon radiation therapy for pediatric brain tumors. J Clin Oncol 34:1043–1049. https://doi.org/10.1200/JCO.2015.62.1383
9. Pulsifer MB, Duncanson H, Grieco J, Evans C, Tseretopoulos ID, MacDonald S et al (2018) Cognitive and adaptive outcomes after proton radiation for pediatric patients with brain tumors. Int J Radiat Oncol Biol Phys 102:391–398. https://doi.org/10.1016/j.ijrobp.2018.05.069
10. Ventura LM, Grieco JA, Evans CL, Kuhlthau KA, MacDonald SM, Tarbell NJ et al (2018) Executive functioning, academic skills, and quality of life in pediatric patients with brain tumors post-proton radiation therapy. J Neurooncol 137:119–126. https://doi.org/10.1007/s11060-017-2703-6

11. Paganetti H (2018) Proton relative biological effectiveness—uncertainties and opportunities. Int J Part Ther 5:2–14. https://doi.org/10.14338/IJPT-18-00011.1
12. Wedenberg M, Toma-Dasu I (2014) Disregarding RBE variation in treatment plan comparison may lead to bias in favor of proton plans. Med Phys 41:91706. https://doi.org/10.1118/1.4892930
13. Paganetti H (2014) Relative biological effectiveness (RBE) values for proton beam therapy. Variations as a function of biological endpoint, dose, and linear energy transfer. Phys Med Biol 59:R419–R472. https://doi.org/10.1088/0031-9155/59/22/R419
14. Yoritsune E, Furuse M, Kuwabara H, Miyata T, Nonoguchi N, Kawabata S et al (2014) Inflammation as well as angiogenesis may participate in the pathophysiology of brain radiation necrosis. J Radiat Res 55:803–811. https://doi.org/10.1093/jrr/rru017
15. Yuan H, Gaber MW, McColgan T, Naimark MD, Kiani MF, Merchant TE (2003) Radiation-induced permeability and leukocyte adhesion in the rat blood–brain barrier: modulation with anti-ICAM-1 antibodies. Brain Res 969:59–69. https://doi.org/10.1016/S0006-8993(03)02278-9
16. Indelicato DJ, Flampouri S, Rotondo RL, Bradley JA, Morris CG, Aldana PR et al (2014) Incidence and dosimetric parameters of pediatric brainstem toxicity following proton therapy. Acta Oncol 53:1298–1304. https://doi.org/10.3109/0284186X.2014.957414
17. MacDonald SM, Laack NN, Terezakis S (2017) Humbling advances in technology: protons, brainstem necrosis, and the self-driving car. Int J Radiat Oncol Biol Phys 97:216–219. https://doi.org/10.1016/j.ijrobp.2016.08.001
18. Roberts KW, Wan Chan Tseung HS, Eckel LJ, Harmsen WS, Beltran C, Laack NN (2019) Biologic dose and imaging changes in pediatric brain tumor patients receiving spot scanning proton therapy. Int J Radiat Oncol Biol Phys 105:664–673. https://doi.org/10.1016/j.ijrobp.2019.06.2534
19. Gunther JR, Sato M, Chintagumpala M, Ketonen L, Jones JY, Allen PK et al (2015) Imaging changes in pediatric intracranial ependymoma patients treated with proton beam radiation therapy compared to intensity modulated radiation therapy. Int J Radiat Oncol Biol Phys 93:54–63. https://doi.org/10.1016/j.ijrobp.2015.05.018
20. Kralik SF, Ho CY, Finke W, Buchsbaum JC, Haskins CP, Shih C-S (2015) Radiation necrosis in pediatric patients with brain tumors treated with proton radiotherapy. AJNR Am J Neuroradiol 36:1572–1578. https://doi.org/10.3174/ajnr.A4333
21. Niemierko A, Schuemann J, Niyazi M, Giantsoudi D, Maquilan G, Shih HA et al (2021) Brain necrosis in adult patients after proton therapy: Is there evidence for dependency on linear energy transfer? Int J Radiat Oncol Biol Phys 109:109–119. https://doi.org/10.1016/j.ijrobp.2020.08.058
22. Paganetti H (2017) Relating the proton relative biological effectiveness to tumor control and normal tissue complication probabilities assuming interpatient variability in α/β. Acta Oncol 56:1379–1386. https://doi.org/10.1080/0284186X.2017.1371325
23. Devine CA, Liu KX, Ioakeim-Ioannidou M, Susko M, Poussaint TY, Huisman TAGM et al (2019) Brainstem injury in pediatric patients receiving posterior fossa photon radiation. Int J Radiat Oncol Biol Phys 105:1034–1042. https://doi.org/10.1016/j.ijrobp.2019.08.039
24. Haas-Kogan D, Indelicato D, Paganetti H, Esiashvili N, Mahajan A, Yock T et al (2018) National Cancer Institute workshop on proton therapy for children: considerations regarding brainstem injury. Int J Radiat Oncol Biol Phys 101:152–168. https://doi.org/10.1016/j.ijrobp.2018.01.013
25. Scharl S, Kirstein A, Kessel KA, Duma M-N, Oechsner M, Straube C et al (2019) Cavity volume changes after surgery of a brain metastasis-consequences for stereotactic radiation therapy. Strahlenther Onkol 195:207–217. https://doi.org/10.1007/s00066-018-1387-y
26. Wald PM, Raval R, Guiou M (2016) Surgical cavity dynamics after resection of brain metastases and its implications for postoperative radiosurgery. Int J Radiat Oncol Biol Phys 96:E93–E94. https://doi.org/10.1016/j.ijrobp.2016.06.827
27. Jarvis LA, Simmons NE, Bellerive M, Erkmen K, Eskey CJ, Gladstone DJ et al (2012) Tumor bed dynamics after surgical resection of brain metastases: implications for postoperative radiosurgery. Int J Radiat Oncol Biol Phys 84:943–948. https://doi.org/10.1016/j.ijrobp.2012.01.067
28. Kraus KM, Heath E, Oelfke U (2011) Dosimetric consequences of tumour motion due to respiration for a scanned proton beam. Phys Med Biol 56:6563–6581. https://doi.org/10.1088/0031-9155/56/20/003
29. Lambert J, Suchowerska N, McKenzie DR, Jackson M (2005) Intrafractional motion during proton beam scanning. Phys Med Biol 50:4853–4862. https://doi.org/10.1088/0031-9155/50/20/008
30. Szeto YZ, Witte MG, van Kranen SR, Sonke J-J, Belderbos J, van Herk M (2016) Effects of anatomical changes on pencil beam scanning proton plans in locally advanced NSCLC patients. Radiother Oncol 120:286–292. https://doi.org/10.1016/j.radonc.2016.04.002
31. Müller BS, Duma MN, Kampfer S, Nill S, Oelfke U, Geinitz H et al (2015) Impact of interfractional changes in head and neck cancer patients on the delivered dose in intensity modulated radiotherapy with protons and photons. Phys Med 31:266–272. https://doi.org/10.1016/j.ejmp.2015.02.007
32. El-Gamal FE-ZA, Elmogy M, Atwan A (2016) Current trends in medical image registration and fusion. Egypt Inform J 17:99–124. https://doi.org/10.1016/j.eij.2015.09.002
33. Eekers DB, In 't Ven L, Roelofs E, Postma A, Alapetite C, Burnet NG et al (2018) The EPTN consensus-based atlas for CT- and MR-based contouring in neuro-oncology. Radiother Oncol 128:37–43. https://doi.org/10.1016/j.radonc.2017.12.013
34. Villemoes E (2018) Volumetric reconstruction and representation with applications in radiotherapy planning. Linkopings Universitet, Department of Physics, Chemistry and Biology
35. Zou KH, Warfield SK, Bharatha A, Tempany CMC, Kaus MR, Haker SJ et al (2004) Statistical validation of image segmentation quality based on a spatial overlap index. Acad Radiol 11:178–189
36. Fleiss J (1981) Statistical methods for rates and proportions, 2nd edn. Wiley, New York, pp 212–236
37. Fedorov A, Beichel R, Kalpathy-Cramer J, Finet J, Fillion-Robin J-C, Pujol S et al (2012) 3D Slicer as an image computing platform for the Quantitative Imaging Network. Magn Reson Imaging 30:1323–1341. https://doi.org/10.1016/j.mri.2012.05.001
38. Fjæra LF, Li Z, Ytre-Hauge KS, Muren LP, Indelicato DJ, Lassen-Ramshad Y et al (2017) Linear energy transfer distributions in the brainstem depending on tumour location in intensity-modulated proton therapy of paediatric cancer. Acta Oncol 56:763–768. https://doi.org/10.1080/0284186X.2017.1314007
39. Acharya S, Wang C, Quesada S, Gargone MA, Ates O, Uh J et al (2021) Adaptive proton therapy for pediatric patients: improving the quality of the delivered plan with on-treatment MRI. Int J Radiat Oncol Biol Phys 109:242–251. https://doi.org/10.1016/j.ijrobp.2020.08.036